Modified Mason number for charged paramagnetic colloidal suspensions

Di Du, Elaa Hilou, and Sibani Lisa Biswal

Phys. Rev. E **93**, 062603 — Published 10 June 2016

DOI: 10.1103/PhysRevE.93.062603

Modified Mason Number for Charged Paramagnetic Colloidal Suspensions

Di Du, Elaa Hilou, Sibani Lisa Biswal

Rice University, Houston, TX

Abstract

The dynamics of magnetorheological fluids have typically been described by the Mason number, a governing parameter defined as the ratio between viscous and magnetic forces in the fluid. For most experimental suspensions of magnetic particles, surface forces, such as steric and electrostatic interactions, can significantly influence the dynamics. Here we propose a theory of a modified Mason number that accounts for surface forces and show that this modified Mason number is a function of interparticle distance. Finally, we demonstrate that this modified Mason number is accurate in describing the dynamics of a rotating pair of paramagnetic colloids of identical or mismatched sizes in either high or low salt solutions. The modified Mason number is confirmed to be pseudo-constant for particle pairs and particle chains undergoing stable-metastable transition during rotation. The interparticle distance term can be calculated using theory or can be measured experimentally. This modified Mason number is more applicable to magnetorheological systems where surface forces are not negligible.

I. Introduction

Paramagnetic colloidal particles suspended in nonmagnetic carrier liquids can undergo rapid and reversible assembly under the application of an external magnetic field [1,2]. This notable feature stems from the fact that under the influence of uniaxial or rotating magnetic fields, the particles acquire magnetic moments, where the induced magnetic interaction leads to the formation of chainlike structures or two-dimensional (2-D) aggregates [3-5]. Regardless of the type of applied magnetic field, the main forces governing the fluid properties are magnetic forces, which effectively bond the particles together, and viscous forces, which try to segment the formed structure. The dimensionless ratio between these two forces, often referred to as the Mason number (*Mn*), governs the mechanical structure of the particles and therefore the rheological properties of the fluid [3,6,7]. However, this number neglects surface forces, such as electrostatic or steric repulsion between particles, which is important because experimental studies typically use paramagnetic colloidal particles that have been functionalized with charged groups or tethered polymers to stabilize the suspension.

The expression of the Mason number can be derived by considering the classic case of two spherical paramagnetic particles suspended in fluid under a rotating magnetic field [3]. By using the dipolar model to calculate the magnetic force between the two spheres, the Mason number is defined as:

$$Mn = \frac{144\pi\eta f}{\mu_0 \chi_1 \chi_2 H_0^2} \tag{1}$$

which has a constant value of 1 when the particle pair undergoes a stable-metastable transition. Here, f is the frequency of the applied field, η is the viscosity of the surrounding fluid, H_0 is the magnitude of the applied field, μ_0 is the vacuum permeability and χ_1, χ_2 are the volumetric susceptibilities of the two particles. This expression only considers magnetic forces and viscous drag and thus cannot be used for paramagnetic suspensions with repulsive surface forces. We propose a theory of a modified Mason number that includes surface forces. With this theory, the stable-

metastable transition frequency observed in rotating chains of paramagnetic colloids can be determined more accurately than the original Mason number. Similar to the Mason number, our modified Mason number is the governing number for the dynamics of particle chains and 2-D clusters.

II. Materials and Methods

A. Sample Fabrication

The particles used in this study are carboxyl-coated superparamagnetic polystyrene particles Dynabeads M-270 and MyOne (Life Technologies). The mean diameters of the particles are 2.8 μm and 1.04 μm, respectively, and effective volumetric magnetic susceptibilities of the beads are 0.96 and 1.4, respectively, as provided by the manufacturer. The particles are suspended in 0.1 mM NaCl or 1 mM NaCl solution. Both particles are negatively charged and have surface potential $\psi_0 = -50$ mV [8,9]. Changing the salt concentration does not significantly change the surface potential. The suspension is confined between two coverslips, which are pretreated with ethyl alcohol and cleaned using a plasma cleaner (Harrick Plasma PDC-32G). The particles settle to the bottom coverslip due to gravity, where the apparent viscosity is different from that in the bulk fluid far from the coverslip[10]. The apparent viscosity is 2.26cP, as measured using passive microrheology by tracking a single particle in the same sample cell. The particles are well-confined in 2-D with a vertical fluctuation that does not exceed 2% of their diameter when the external magnetic field is on, as measured by a three-axis piezo-controller (Newport ESA-C).

B. Magnetic and Imaging Setup

The sample cell is placed on a horizontal sample holder at the center of an orthogonal set of air-core solenoids (Fig. 1). The applied magnetic field can be expressed using the vector form $\mathbf{H_0} = \left(H_0 \cos(2\pi ft), H_0 \sin(2\pi ft)\right)$, where H_0 is the magnetic field strength, f is frequency and t is the elapsed time. Two multi-frequency power supplies, which are

connected to the two coil pairs (Agilent N6784A), are programmed with orthogonal sinusoidal functions to generate a rotating magnetic field. The instantaneous voltage from the power supply to the coils is monitored using a digital oscilloscope. The applied magnetic field strength is calculated using a correlation between magnetic field strength and applied voltage, as determined using a Gauss meter (AlphaLab GM1-HS). The particles are tracked using a 100x/1.4 Olympus oil objective beneath the sample holder combined with a CCD camera (QImaging QICam).

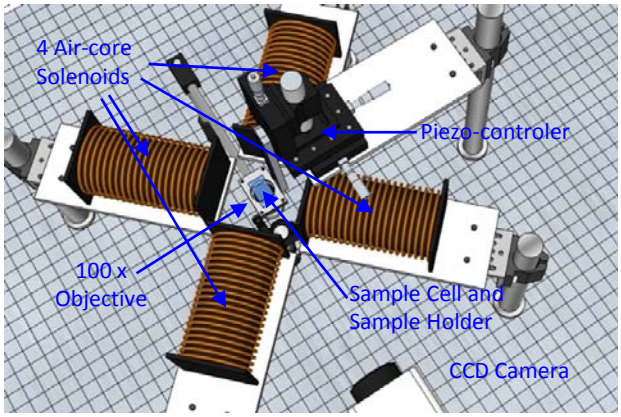

Fig. 1 Schematic view of the experimental setup.

III. Results and Discussions

A. A Particle Pair under a Rotating Magnetic Field

Under a rotating magnetic field of 10 Oe, at low field frequency ($f_H \leq 0.46$ Hz), a particle pair rotates synchronously with the external field, and its sweep angle follows the simple multiplication $\phi = 360$ ft degree with a linear increase (Fig. 2(a)). Further increasing f_H above 0.46 Hz leads to a phase lag between the particle pair and the external field larger than a critical value above which the force between two paramagnetic particles is repulsive, which results in the particle pair intermittently rotating reversely and realigning with the external field and therefore a smaller sweep angle [11]. The reverse rotation occurs more frequently as f_H is further increased, leading to even smaller sweep angles. Therefore, at $f_H = 0.46$ Hz, the particle pair reaches the

largest rotating frequency $f_P = 0.46\ Hz$, as shown in Fig. 2(b). The reverse rotation is better visualized using the trajectory of either particle. The insets of Fig. 2(b) compare the trajectories from $f_H = 0.46\ Hz$ and $f_H = 0.47\ Hz$. The former state features a smooth circular trajectory and the latter a circular trajectory with 6 knots, corresponding to the 6 kinks on the blue curve in Fig. 2(a). Thus, $f_H \leq 0.46\ Hz$ is often referred to as the stable region and $f_H > 0.46\ Hz$ as the metastable region. This stable-metastable transition occurs at different transition frequencies f_t for different external field strengths.

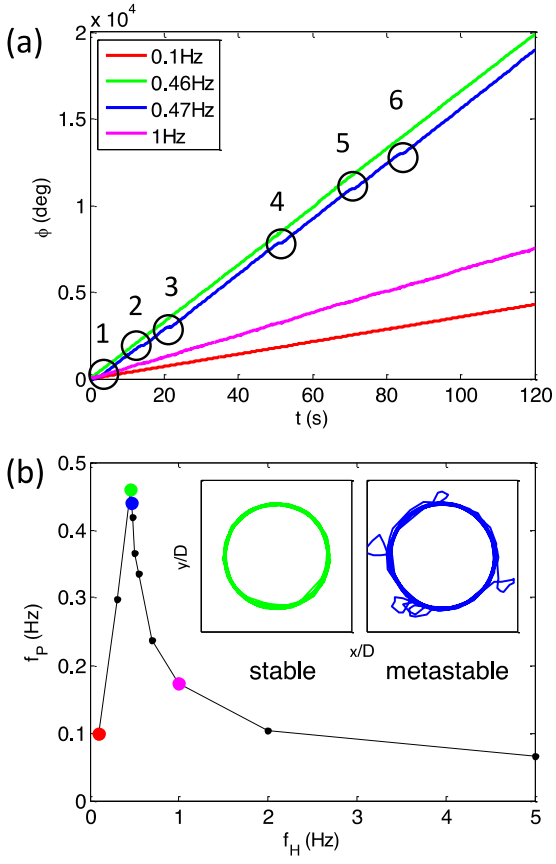

Fig. 2 The rotation dynamics of a pair of M-270 particles (2.8 μm) in 0.1 mM NaCl solution under a 10 *Oe* rotating magnetic field. (a) Sweep angle of the pair over time at different external field frequencies. (b) The rotating frequencies of the pair as a response to different frequencies of the rotating field. The 4 colored markers correspond to the 4 different sweep angle curves in (a). Insets show the trajectories of one particle for the stable ($f_H = 0.46\ Hz$, green) and metastable ($f_H = 0.47 Hz$, blue) states.

B. Derivation of the Modified Mason Number

The metastable particle pair is directly caused by the phase lag, which is the angle between the applied magnetic field $\mathbf{H}_0$ and the connector vector between two particles $\mathbf{r}$. The phase lag significantly affects the force balances on both particles symmetrically. The force balance on particle 2 is shown in Fig. 3(a) with phase lag α. Here, $\mathbf{F}_\mathrm{m}$, $\mathbf{F}_\mathrm{e}$ and $\mathbf{F}_\mathrm{v}$ are the magnetic force, electrostatic force and viscous drag, respectively, and $\hat{\mathbf{r}}$ and $\hat{\boldsymbol{\alpha}}$ are unit vectors in the radial and azimuthal directions, respectively. We use dipolar model [12] to describe the magnetic force

$$\mathbf{F}_\mathrm{m} = -\frac{\mu_0 \pi H_0^2 d_1^3 d_2^3 \chi_1 \chi_2}{12 r^4}\left[(3\cos^2\alpha - 1)\hat{\mathbf{r}} + 2\sin\alpha\cos\alpha\hat{\boldsymbol{\alpha}}\right] \tag{2}$$

where r is the distance between the two particles, and μ_0 is the vacuum permeability. DLVO theory [13] and Stokes' law are adopted to calculate the electrostatic repulsion and viscous drag, respectively:

$$\mathbf{F}_\mathrm{e} = (32\pi k T d_h \rho_\infty \gamma^2 / \kappa^2) e^{-\kappa(r-d_a)}\hat{\mathbf{r}} \tag{3}$$

$$\mathbf{F}_\mathrm{v} = (3\pi^2 \eta d_h r f)\hat{\boldsymbol{\alpha}} \tag{4}$$

For Eqn. (3), $d_h = \dfrac{2d_1 d_2}{d_1 + d_2}$ is the harmonic mean of the particle diameters, $d_a = \dfrac{d_1 + d_2}{2}$ is the arithmetic mean of the particle diameters, ρ_∞ is the number density of ions in the bulk solution, κ is the reciprocal of the Debye length, and $\gamma = \tanh(ze\psi_0 / 4k_B T)$ is the reduced potential, where ψ_0 is the surface potential and e is the unit charge. For Eqn. (4), η is the viscosity of the fluid, and f is the field frequency. At any f before the transition, both particles undergo constant circular motion, and the net force on particle 2 is zero when inertia is neglected. Therefore, we have $\mathbf{F}_\mathrm{m}\cdot\hat{\mathbf{r}} + \mathbf{F}_\mathrm{e}\cdot\hat{\mathbf{r}} = 0$ and $\mathbf{F}_\mathrm{m}\cdot\hat{\boldsymbol{\alpha}} + \mathbf{F}_v\cdot\hat{\boldsymbol{\alpha}} = 0$. After rearranging terms and lumping them into dimensionless groups, these two equations become:

$$Mn \cdot R^5 = \sin(2\alpha) \tag{5}$$

$$\lambda R^4 e^{(1-R)\xi} = 3\cos^2\alpha - 1 \tag{6}$$

Here, $R = r/d_a$ is normalized center-to-center distance, $\lambda = \frac{1536kTd_h\rho_\infty\gamma^2/\kappa}{\mu_0\chi_1\chi_2H_c^2(d_g/d_a)^4d_a^2}$ is the ratio between electrostatic force and magnetic force, $Mn = \frac{144\pi\eta f}{\mu_0\chi_1\chi_2H_0^2(d_g/d_a)^4}$ is the Mason number considering particle size difference, $\xi = \kappa d_a$ is the normalized Debye length and $d_g = \sqrt{d_1d_2}$ is the geometric mean of the particle diameters. When the particles have no surface charge, λ vanishes and $\alpha_t = \arccos\frac{1}{\sqrt{3}}$ from Eqn. (6). Before the transition, R = 1 and α increases with increasing frequency, or Mn from Eqn. (5). The particle pair undergoes a stable-metastable transition when Mn reaches a maximum and α reaches the magic angle [14] $\arccos\frac{1}{\sqrt{3}}$, where neither particle experiences a radial force. Here because the surface charge is included, both R and α increase with increasing Mn. Likewise, Mn reaches a maximum at the transition point because Mn is only a function of f, and they both reach maxima for a given particle pair undergoing the transition. Combining Eqn. (5) and (6), we can cancel out α and obtain the expression for Mn:

$$Mn(R) = \frac{\sqrt{1-\frac{4}{9}\left(\lambda R^4 e^{-\xi R} - \frac{1}{2}\right)^2}}{R^5} \tag{7}$$

Fig. 3(b) shows how Mn changes with increased R from Eqn. (7) for a pair of M-270 particles in 0.1 mM NaCl solution under a 10 *Oe* rotating magnetic field. As R increases, Mn first increases to its maximum and then gradually decreases. Before Mn reaches the maximum M, the rotation of the pair is stable and follows the rotation of the external field. After Mn starts to drop, the rotation of the pair is unstable and quickly moves towards the stable state with the same Mn but a small R on the left of M. Therefore, the unstable state on the right of M does not physically exist, and the metastable state is observed instead, which is shown by the magenta markers. When Mn reaches a maximum,

its slope, $\frac{dMn(R_t)}{dR_t}$=0. It is difficult to obtain an analytical expression for R_t, but one of the iterative expressions for R_t is

$$R_t = \frac{\ln\left[\frac{\lambda}{16} R_t^4 \left(\sqrt{(6+\xi R_t)^2 + 64(1+\xi R_t)} - (6+\xi R_t)\right)\right]}{\xi} + 1 \tag{8}$$

For short range repulsive surface forces, such as electrostatic forces, the interaction potential formed from the repulsive interaction and attractive magnetic interaction confines the particle separation to be very small compared to the particle size. Thus, R is very close to 1. Starting from an initial guess of 1, the change of the left hand side of Eqn. (8) does not exceed 0.1% after two iterations. The transition frequency f_t can be obtained using

$$f_t = \frac{Mn_t \cdot \mu_0 \chi_1 \chi_2 H_0^2 (d_g / d_a)^4}{144\pi\eta} \tag{9}$$

where Mn_t is obtained using Eqn. (7).

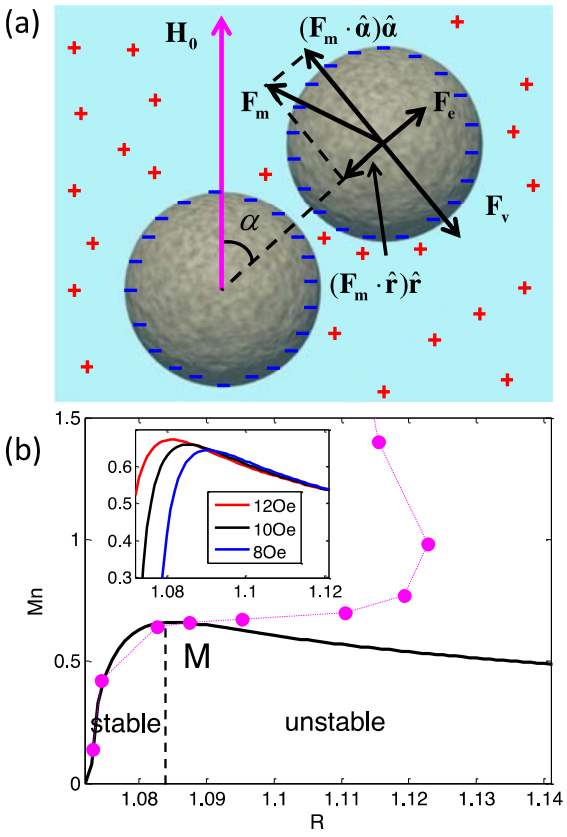

Fig. 3 (a) The forces exerted on a paramagnetic particle of a particle pair. (b) The Mason number *Mn* as a function of normalized center-to-center distance *R* for a pair of M-270 particles in 0.1 mM NaCl solution under a 10 *Oe* rotating magnetic field. The magenta markers correspond to experimental measurements fit to Eqn. (1), and the black curve corresponds the expression calculated by Eqn. (7). M is the maximum of *Mn* predicted by Eqn. (7), and the vertical dashed line across M is the boundary between the stable and unstable region. The inset shows the same profile for different external field strengths.

The Mn_t obtained from Eqn. (7) changes when different external field strengths are used (Fig. 3(b) inset). The f_t obtained from Eqn. (9) is therefore different from the predicted value from the original Mason number definition. Fig. 4(a) ~ (d) compares the transition frequency, f_t, calculated from the original Mason number theory predicted by Eqn. (9), which includes electrostatic forces and that obtained from experiments for different particle sizes and salt concentrations. For all experiments, Eqn. (9) matches the experimental results. For the case of two mismatched sized particles suspended at low

salt concentrations, there is a slight deviation between the predicted and experimentally observed f_t due to the stochastic forces from the surrounding fluid, which play a larger role at lower magnetic field strengths. The inset of Fig. 3(b) shows that *Mn* is not constant at the stable-metastable transition, which indicates that *Mn* is not the governing number for the dynamics of the system.

Martin *et al* [3], showed that for a particle pair that considers the magnetic and viscous torques, the stable-metastable transition occurs at a transition phase lag $\alpha_t = \arccos\frac{1}{\sqrt{3}}$. For a particle pair with electrostatic repulsion, $\sin(2\alpha_t)$ is approximately 1, with a deviation that does not exceed 10^{-4} when the external field strength changes from 8 *Oe* to 28 *Oe*. Hence, when electrostatic repulsion is considered, $\sin(2\alpha_t)$ can be considered a pseudo-constant or α_t=45°. Our modified Mason number is

$$Mn' = Mn \cdot R^5 \tag{10}$$

which accounts for how short-range surface forces change R.

C. Application of the Modified Mason Number on Particle Pairs

Systematic experiments on the rotation dynamics of a particle pair are conducted to verify the definition of Mn' and compare it with the hard sphere system described by the original theory of the Mason number. Fig. 4(e) shows the change of the rotating frequency of the particle pair as a function of Mn'. This is essentially the same profile as Fig. 2(c), except that the x-axis is replaced by the modified Mason number, and the y-axis is scaled by the transition frequency under specific conditions. Different colors represent the different external magnetic field strengths used in Fig. 4(a-d). All data points fall onto a master curve, which confirms that Mn' is the governing number for the rotation dynamics of a particle pair. Note that the Mn's are calculated using experimentally measured interparticle distances to validate the definition of Mn'. The experimentally measured interparticle distance matches Eqn. (7) in the stable region, as shown in Fig. 3(b); therefore, using Eqn. (7) does not cause noticeable differences when calculating Mn'. Thus, the pseudo-constant modified Mason number can be combined with Eqn. (7) to predict the distance between a pair of paramagnetic particles suspended in fluid when it is not easy to measure.

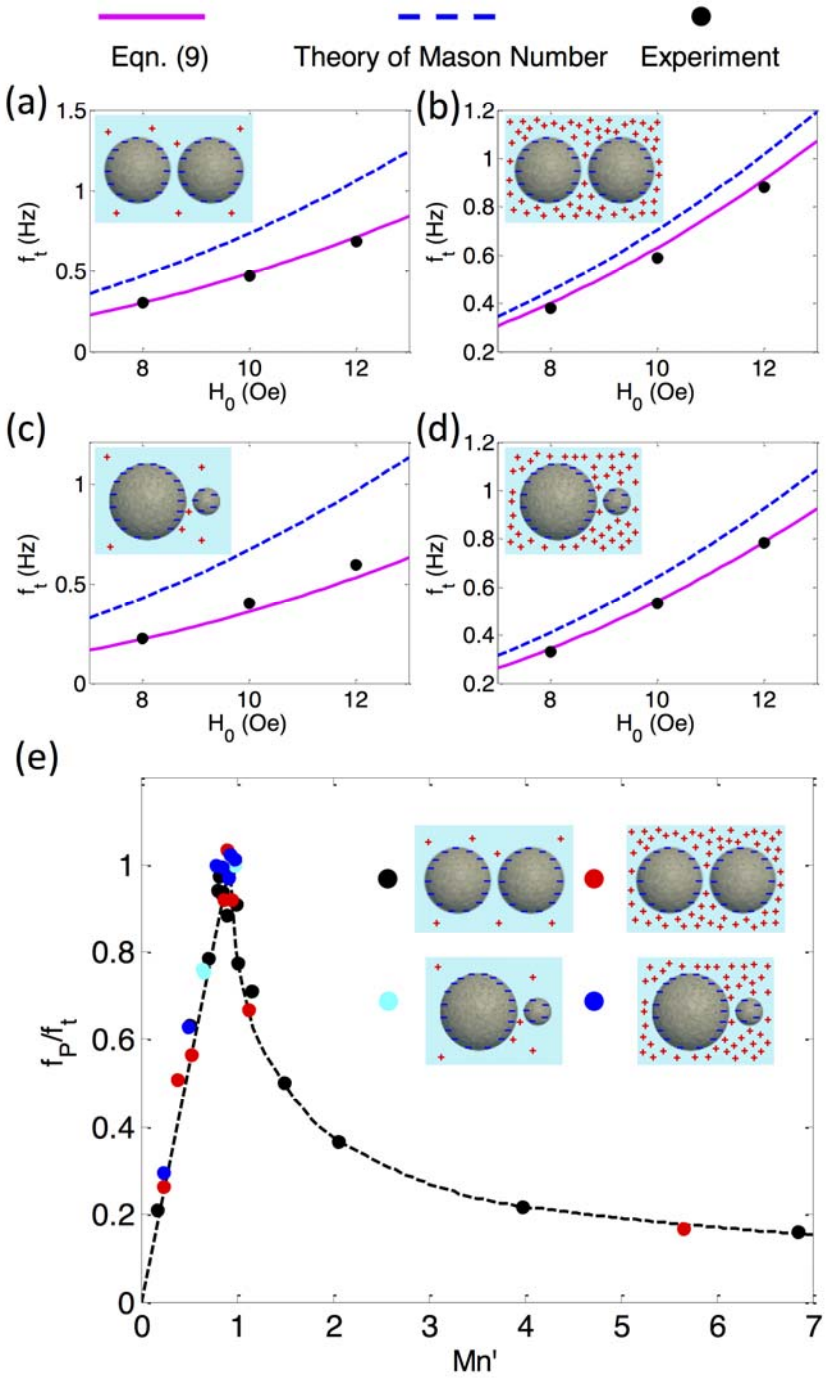

Fig. 4 The transition frequency of a dimer for different field strengths. (a) 2.8 μ*m* and 2.8 μ*m*, 0.1 mM NaCl, (b) 2.8 μ*m* and 2.8 μ*m*, 1 mM NaCl, (c) 2.8 μ*m* and 1.04 μ*m*, 0.1 mM NaCl, (d) 2.8 μ*m* and 1.04 μ*m*, 1 mM NaCl. (e) When the particle rotation frequency is normalized by the transition frequency and plotted against the modified Mason number,

the experiments collapse onto a single master curve. The black, red, cyan and blue markers correspond to conditions (a) ~ (d), respectively. The dashed line is a trendline for the modified Mason number.

D. Application of the Modified Mason Number to Particle Chains

The theory of the modified Mason number can be extended to a chain of particles. We consider a chain made of particles of the same size. Similar to a particle pair, a particle chain first rotates synchronously and then asynchronously with the rotating field when frequency is increased. When a chain transitions into asynchronous rotation, it will fragment into two pieces at or near the center of rotation, rotate and eventually reform into a chain [15]. For a three-particle chain, since one of the two fragments is a single particle, the two fragments may quickly reform a chain *in situ* without any effective rotation of the fragments. The trajectory of the single particle will form a knot similar to that of a particle in a pair shown in Figure 2(b). Note that for the chain experiments, the larger particles are used to limit the influence of stochastic forces from the surrounding fluid, which could trigger chain fragmentation prior to the synchronous-asynchronous transition.

When placed in a rotating magnetic field, the azimuthal constraint of a particle chain rotating synchronously with external field is given by the balance between the hydrodynamic torque and magnetic torque along the chain. We analyze torques on only half of the chain due to symmetry. The highest hydrodynamic torque along the chain is exerted on the central particle, with expression [3]

$$\tau_h = 3\pi^2 \eta f d r^2 (N/2)^2 \tag{11}$$

The magnetic torque on the central particle is given by

$$\tau_m = -\frac{\zeta \mu_0 \pi \chi^2 d^6 H_0^2}{24 r^3} \sin(2\alpha) \tag{12}$$

where $\zeta = 1+2\sum_{n=2}^{\lfloor N/2 \rfloor+1} \frac{1}{n^3}$ is similar to the Riemann zeta function, but with a finite truncation, and $\lfloor x \rfloor$ gives the largest integer smaller than or equal to x. The dipolar model uses ζ to account for the magnetic interaction further than the nearest neighbors. At the fragmentation transition frequency, the two torques are counterbalanced with a constraint $Mn'_t = \frac{2\zeta \sin(2\alpha_t)}{(N/2)^2}$. The radial constraint can be given similarly to that of a particle pair by $\lambda R^4 e^{(1-R)\xi}/\zeta = 3\cos^2\alpha - 1$. Likewise $\sin(2\alpha_t)$ is found pseudo-constant or α_t=45°. Therefore, we obtain

$$\frac{1}{Mn'_t} = \frac{N^2}{8\zeta} \tag{13}$$

Compared to $\frac{1}{Mn_t} = \frac{3\sqrt{2}N^2}{32}$ for systems without surface forces [3], the difference in the prefactor in Eqn. (12) is a result of different phase lag angles upon transition as a result of electrostatic repulsion. Fig. 5 shows the comparison among experimental measurements of Mn_t and Mn'_t for chains consisting of M-270 particles in 0.1 mM NaCl solution. The experimentally measured $\frac{1}{Mn'_t}$ matches the calculation given by Eqn. (13). The experimental results for $\frac{1}{Mn_t}$ significantly deviate from both Eqn. (13) and $\frac{1}{Mn_t} = \frac{3\sqrt{2}N^2}{32}$. Unlike for a particle pair, the Mason number does not change much when the external field strength is changed for a particle chain because the chain configuration buffers the change of the interparticle distance compared to a particle pair under the same external field strengths. A larger external magnetic field strength leads to smaller interparticle distances between particles, which cause an exponential increase in the electrostatic forces as particles are brought closer together.

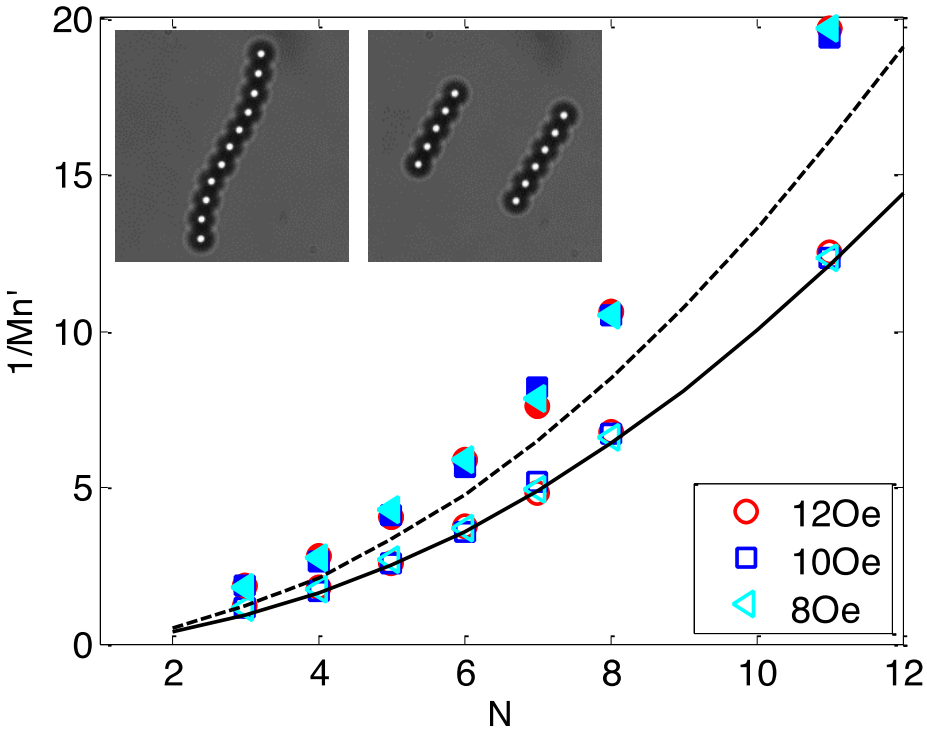

Fig. 5 The Mason number and modified Mason number for fragmentation transition of chains of M-270 particles (2.8 μ*m*) in 0.1 mM NaCl solution. The solid markers correspond to the reciprocal of the Mason numbers and the hollow markers correspond to the reciprocal modified Mason number. The solid line corresponds to Eqn. (13), and the dashed line corresponds to $\frac{3\sqrt{2}N^2}{32}$. The insets show the snapshots of the experiment before and after a particle chain fragments.

E. Degrees of Freedom

The modified Mason number Mn' can be used to better predict the dynamics of systems consisting of suspended paramagnetic colloids with surface forces because it considers one additional degree of freedom from how surface forces alter interparticle distances. The interparticle distance is primarily dependent on the balance between the magnetic and surface forces. The dependence on the magnetic force can be independently decomposed into applied field strength and phase lag if the particle properties are fixed.

Therefore, Eqn. (8) can be used to delineate the dependence of the interparticle distance on the magnetic field strength.

Because the repulsive surface forces are always short-ranged, R_t is close to 1 even if the frequency or the strength of the external magnetic force significantly changes. Changing R_t yields a more significant change in R_t^4 than $\sqrt{(6+\xi R_t)^2+64(1+\xi R_t)}-(6+\xi R_t)$ in Eqn. (8). Therefore, an approximation $R_t \approx \frac{\ln\left[\frac{\lambda}{16}R_t^4\left(\sqrt{(6+\xi)^2+64(1+\xi)}-(6+\xi)\right)\right]}{\xi}+1=\frac{\ln\left(\frac{A}{H_0^2}R_t^4\right)}{\xi}$ can be made. Here, a constant $A=\frac{96kTd_h\rho_\infty e^{\xi}\gamma^2/\kappa}{\mu_0\chi_1\chi_2(d_g/d_a)^4 d_a^2}\left(\sqrt{(6+\xi)^2+64(1+\xi)}-(6+\xi)\right)$ is defined after H_0 is extracted from λ. Because $\ln R_t \approx 0$, $R_t \approx \frac{\ln\left(\frac{A}{H_0^2}R_t^4\right)}{\xi} \approx \frac{\ln\left(\frac{A}{H_0^2}\right)}{\xi}$. Therefore, we can define the modified Mason number when the measurement on R_t is difficult to obtain:

$$Mn''_t = Mn_t \cdot \left[\ln\left(\frac{A}{H_0^2}\right)/\xi\right]^5 = \frac{144\pi\eta f\left[\ln(A/H_0^2)\right]^5}{\mu_0\chi_1\chi_2 H_0^2(d_g/d_a)^4\xi^5} \quad (14)$$

This definition only takes into account the dependence of interparticle distance on the applied field strength; therefore, its value upon transition might not be equal to 1. The modified Mason number defined in Eqn. (14) is pseudo-constant for a certain structure but is different for different structures (Fig. 6). Structures formed from particles with monodisperse size have values close to 1, whereas structures formed from particles with mismatched size have values as small as 0.6.

Although the measurement of interparticle distance is no longer required, another degree of freedom is involved due to the variant value of the modified Mason number for different structures. The additional degree of freedom requires accurate measurements on one more parameters, which is challenging for smaller particles [8].

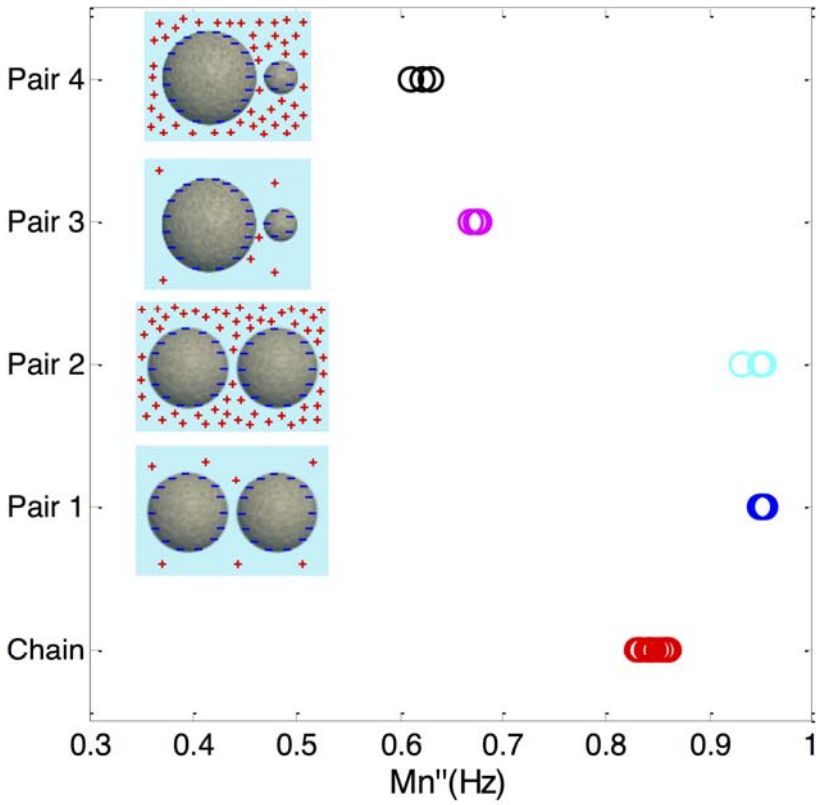

Fig. 6 The modified Mason number from Eqn. (14). Pairs 1~4 correspond to the configurations in Figs. 4(a) ~ (d), respectively. Data obtained at 8 *Oe*, 10 *Oe* and 12 *Oe* are superimposed for each structure. For the particle chain, Mn''_t is scaled by $\frac{8\zeta}{N^2}$.

IV. Conclusion

We describe how to modify the definition of the Mason number to consider surface forces in magnetorheological fluids. This theory is based on the fact that a modified Mason number is pseudo-constant and is therefore able to predict the stable-metastable transition of a particle pair. For comparison, the original Mason number definition does predict the dynamics of a particle pair, especially at low salt concentrations, where electrostatic repulsion between particles is relatively large. Our modified Mason number is better able to capture the dynamics of different structures formed by paramagnetic particles under a rotating magnetic field, including pairs and chains. It involves an additional degree of

freedom and thus requires the measurement of one additional parameter, such as the interparticle spacing.

Although the theory derived here is for electrostatic forces, it is applicable to other types of surface forces with modification to the ratio between the surface and magnetic forces. Additionally, the modified Mason number can be used to predict the rheological behavior of magnetorheological fluids in a variety of shear flows that involve the breaking and reforming of chains of particles in the fluid [3].

Acknowledgement

We gratefully thank Steve Kuei for his insightful discussions. Funding for this research was provided by the National Science Foundation under award number CBET-0955003.

References

[1] B. J. Park, F. F. Fang, and H. J. Choi, Soft Matter **6**, 5246 (2010).

[2] S. Genc and P. P. Phule, Smart Mat. Struct. **11**, 140 (2002).

[3] S. Melle and J. E. Martin, J. Chem. Phys. **118**, 9875 (2003).

[4] E. M. Furst and A. P. Gast, Phys. Rev. E **61**, 6732 (2000).

[5] S. Melle, O. G. Calderón, M. A. Rubio, and G. G. Fuller, Phys. Rev. E **68**, 041503 (2003).

[6] O. G. Calderon and S. Melle, J. Phys. D-Appl. Phys. **35**, 2492 (2002).

[7] D. J. Klingenberg, J. C. Ulicny, and M. A. Golden, J. Rheol. **51**, 883 (2007).

[8] D. C. Li, C. N. Lam, and S. L. Biswal, Soft Matter **6**, 239 (2010).

[9] D. Du, D. Li, M. Thakur, and S. Biswal, Soft Matter **9**, 6867 (2013).

[10] M. A. Bevan and D. C. Prieve, J. Chem. Phys. **113**, 1228 (2000).

[11] See Supplemental Material at http://link.aps.org/supplemental/XXX for a movie of a particle pair rotating asynchronously with external field.

[12] E. E. Keaveny and M. R. Maxey, J.Comp. Phys. **227**, 9554 (2008).

[13] J. Israelachvili, Intermolecular and Surface Forces. (Academic Press, San Diego, CA, 1992).

[14] N. Osterman, I. Poberaj, J. Dobnikar, D. Frenkel, P. Ziherl, and D. Babic, Phys.

Rev. Lett. **103**, 4 (2009).

[15] See Supplemental Material at http://link.aps.org/supplemental/XXX for a movie of the fragmentation of a chain of 11 particles.